

Thermal Design of Linear Induction and Synchronous Motors for Electromagnetic Launch of Civil Aircraft

Luca Bertola, Tom Cox, *Member, IEEE*, Pat Wheeler, *Senior Member, IEEE*, Seamus Garvey, and Herve Morvan

Abstract—The engine size of modern passenger transport aircraft is principally determined by take-off conditions, since initial acceleration requires maximum engine power. An electromagnetic launch (EML) system could provide some or all of the energy required at takeoff so that the aircraft engine power requirement and fuel consumption may be significantly reduced. So far, EML for aircraft has been adopted only for military applications to replace steam catapults on the deck of aircraft carriers. This paper will describe the potential application of EML to propel civil aircraft on the runways of modern airports. A comparison of synchronous and asynchronous electrical motor systems designed to launch an A320-200 sized aircraft is presented. The paper also describes a solution of the transient heat transfer problem applied to the conductive components of EML systems.

Index Terms—Civil aircraft, electromagnetic launch (EML)/EMLs, electromagneticcatapult, linear inductionmotor, linear synchronous motor, thermal analysis.

I. INTRODUCTION

THIS paper considers the feasibility of different linear motor technologies for an electromagnetic launch (EML) system to assist civil aircraft takeoff. The thrust level that can be delivered by an EML system allows for accelerations that cannot be reached by aircraft engines. The increased acceleration provided by EML systems has the potential to reduce the nominal runway length required by the aircraft at takeoff.

The machine topologies mainly considered for EML are a double-sided linear induction motor (LIM) [1], a double-sided tubular induction motor [2], and a linear permanent magnet synchronous motor (LPMSM) [3]. In order to achieve the high thrust requirement for aircraft launch applications these machines need to operate with a high current density. Most

Manuscript received December 23, 2016; revised April 7, 2017; accepted April 18, 2017. This work was supported by the People Programme (Marie Curie Actions) of the European Union's Seventh Framework Programme (FP7/2007-2013) under REA Grant 608322. (*Corresponding author: Luca Bertola.*)

L. Bertola is with the Institute for Aerospace Technology, The University of Nottingham, Nottingham NG7 2TU, U.K. (e-mail: luca.bertola@nottingham.ac.uk).

T. Cox and P. Wheeler are with the Department of Electrical and Electronic Engineering, The University of Nottingham, Nottingham NG7 2RD, U.K.

S. Garvey and H. Morvan are with the Department of Mechanical, Materials and Manufacturing Engineering, The University of Nottingham, Nottingham NG7 2RD, U.K.

Color versions of one or more of the figures in this paper are available online at <http://ieeexplore.ieee.org>.

Digital Object Identifier 10.1109/TPS.2017.2697941

TABLE I

COMPARISON BETWEEN MILITARY AND CIVIL REQUIREMENTS FOR EML

Requirements	Jet Aircraft [7]	A320-200
End speed	67.0 m/s	85.7 m/s
Aircraft mass	45000 kg	73500 kg
Acceleration	>2.4 G	0.6 G
Peak Thrust	1074.5 kN	502.9 kN
Runway length	94 m	624 m
Acceleration time	2.80 s	14.57 s

of the electrical machines used for continuous operation with similar rated current densities need an active cooling system for the conductive components [4]. High current densities can be exploited in EML systems for the very short duty cycle of the machines, although an active cooling system may be required to cope with the temperature rise after multiple launches. This paper investigates the temperature-time evolution inside electromagnetic launchers in order to evaluate the possibility to adopt only passive cooling techniques.

In the past, detailed thermal analysis of induction motors has been carried out for rotary machines [5], while this paper focuses on the transient temperature variation on the active area of the conductive plate of the linear counterpart. The thermal analysis of a LPMSM deals with the eddy current losses into the magnets of the synchronous machine and the consequent limits on armature excitation to avoid demagnetization during operation. The temperature variation of the stator coils under the rated current density has been investigated for both linear machine topologies.

The thermal analysis considers the practical thermal limits of the machine topologies, and how these are best exploited in a very short-term rated application such as civil aircraft launching.

II. LAUNCHER REQUIREMENTS

General Atomics developed an EML system that is able to launch jet aircraft as heavy as the F-35C [6]. Table I compares the requirements for the military catapult [7] with those for the launch of an A320-200 aircraft.

The end-speed design requirement for the civil aircraft launcher reported in Table I was established considering a safety margin with respect to the speed at which the aircraft detaches. Since the catapult is connected to the front landing gear, the mover disconnects when the aircraft reaches the

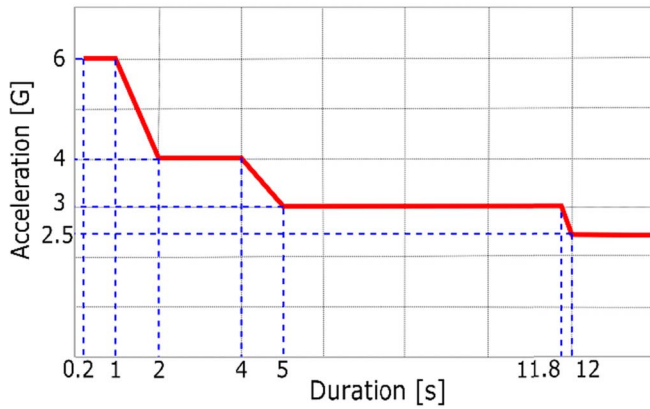


Fig. 1. Axial acceleration limit for a healthy passenger seated with backrest and headrest.

nose rotation speed. The nose rotation speed is the minimum reference speed for the pilot to raise the nose landing gear. The nose rotation speed of the aircraft was determined considering aerodynamic performance which allows the aircraft to safely take off in one engine inoperative conditions.

This means that even when an engine fails during the take-off procedure, the catapult provides enough speed to allow the aircraft to lift off and maneuver to enable an emergency landing. The engine thrust decrease caused by the temperature under hot-day conditions is also considered to calculate the exact moment when the nose rotation speed is reached. Under the combinations of most disadvantageous environmental and operational conditions the nose rotation speed is about 74.5 m/s [8]. Considering a safety factor of 1.15 the design catapult end-speed in Table I is obtained.

The acceleration intensities delivered by an EML system must not jeopardize safety and comfort of the passengers, irrespective of their physical condition and age. Most civil aircraft accelerates up to 0.3 G since the engines thrust peak is about 30%–35% of the maximum take-off weight. The axial acceleration intensity that a healthy person can withstand for a specific time span is shown in Fig. 1. This chart is valid only for an axial acceleration acting perpendicularly to the chest of a passenger seated with backrest and headrest [9].

The duration of the take-off procedure is expected to exceed 12 s which allows a maximum axial acceleration of 2.5 G according to the curve shown in Fig. 1. In order to take into account all the possible health conditions and ages of the passengers, less than the 50% of the maximum limit should be considered (<1.25 G). Besides passenger safety, the comfort of the passengers plays an important role in the selection of an appropriate acceleration level. Independently of the maximum acceleration that can be withstood, every passenger differently perceives acceleration according to personal and psychological factors. Since discomfort may be caused by low accelerations as well, the rated acceleration considered in this work is conservatively assumed to be 0.6 G. This acceleration guarantees passengers safety and comfort even though it exceeds the usual engines acceleration peak.

The increased acceleration and the consequent reduction of the runway length required at takeoff is one of the major

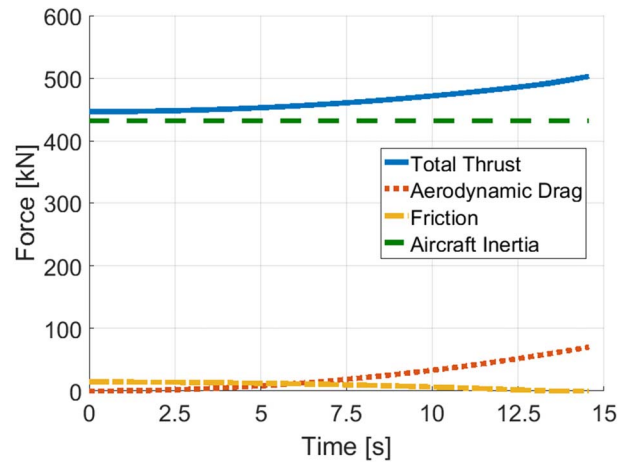


Fig. 2. Variation of the total thrust and thrust components during the launch.

benefits of EML systems. Expensive airport extensions could be avoided by allowing large aircraft to operate from short runways at small airports. Actual runways could respond to air traffic growth through the implementation of an electromagnetic catapult allowing the takeoff of two aircraft simultaneously from the center of the runway accelerating in opposite directions. With a foreseen installation cost of approximately £700 million, an EML system is cheaper than the total expense that is required for the construction of a third runway in Heathrow (£17.6 billion [10]) or for the runway extension (£14.4 billion [10]).

The electromagnetic catapult has to provide the same acceleration rate during the whole take-off procedure overcoming the aerodynamic drag and the friction with the runway pavement. The instantaneous thrust F can be estimated as

$$F = 0.6G \cdot m_{A320} + D + \mu(m_{A320} \cdot G - L) \quad (1)$$

where m_{A320} is the mass of the aircraft reported in Table I, μ is the friction coefficient with the ground (0.02 for a paved runway), and D and L are the aerodynamic drag and lift that can be, respectively, computed as

$$D = \frac{1}{2} \rho_{\text{Air}} S_w C_D v^2 \quad (2)$$

$$L = \frac{1}{2} \rho_{\text{Air}} S_w C_L v^2 \quad (3)$$

where ρ_{Air} is the air density, S_w is the wing surface (approximately 122 m²), v is the speed of the aircraft, C_L is the lift coefficient (approximately 2.22), and C_D is the drag coefficient (approximately 0.127).

The thrust profile needed to accelerate a fully loaded A320-200 aircraft to the required speed and the respective thrust components are shown in Fig. 2. Since the aerodynamic drag grows with the square of the aircraft velocity, the maximum thrust which is reported in Table I is delivered when the aircraft reaches the maximum speed.

The EML of civil aircraft will allow a reduction in the power required from the engines during initial acceleration which has the potential of reducing the aircraft fuel consumption and exhaust emission at ground level. The take-off analysis

estimates 48.6 kg of fuel saving at each takeoff for the reduced usage of the engines [8]. Since the A320-200 engines consume 248.4 kg of fuel at takeoff, the exhaust emission at ground level will decrease by 19.6%. Exploiting the high level of thrust available from an electromagnetic catapult, the engine thrust requirement may be reduced of approximately 8%. With lower thrust requirements, the engine size can be reduced leading to a decrease of the aircraft aerodynamic drag and weight. The new propulsion system configuration would lead to 457 kg of fuel saving across the whole flight and to 20.8% exhaust emission reduction at ground level [8].

Since an electrical motor with zero nominal noise emission is responsible of providing the required energy to accelerate the aircraft at takeoff, an EML system can significantly reduce noise at the airport. Through the implementation of this system, active engines are only needed at the end of the runway, just before starting the climbing phase. Aircraft engines usually take 4 s to pass from the idle condition to maximum power. Comparing the time that the engines spend a full power between conventional and assisted takeoff, approximately 66% noise emission reduction at ground level may be expected [8].

III. ELECTROMAGNETIC DESIGN OF LIM AND LPMSM

The electromagnetic performance of the asynchronous launcher was estimated on the basis of the equivalent circuit model of LIMs [11]. The classic equivalent circuit of rotary induction motor was modified to take into account specific LIM phenomena like end effects and edge effects. Using an additional impedance in parallel with the magnetization inductance in the equivalent circuit of rotary induction motors, the dynamic behavior of the linear machine is well represented.

The LPMSM was sized with the aid of the d-q phasor model and applying the multilayer theory (MLT) [11]. Once the number of poles and the winding distribution of the synchronous machine are defined, the MLT allows the reconstruction of the magnetic flux across the motor as well as the computation of the magnetizing inductance. The dynamic action of the fundamental electromotive force of LPMSM is well estimated by the d-q phasor model.

The selection of the geometrical parameters of the LIM and LPMSM is based on a numerical procedure that iterates the equivalent circuit model and the d-q phasor model, respectively, to find the best motor design which is in compliance with the requirements.

The numerical approach that was adopted is based on the sensitivity analysis of the system which determines the impact of the design variables on the model outcomes. The sensitivity analysis allows for a deeper understanding of the relationships between inputs and outputs finding regions in the space of the design variables where the design objectives meet an optimum criterion (including maximization and minimization problems). Sensitivity analysis is particularly suitable to identify the way a model with a large number of parameters “senses” the variations of some design inputs.

This numerical method is performed by running a mathematical model a large number of times for each combination

TABLE II
COMPARISON BETWEEN ELECTROMAGNETIC PERFORMANCE AND GEOMETRICAL FEATURES OF LIM AND LPMSM

Parameter	LIM	LPMSM
Peak Efficiency	0.926	0.986
Power Factor	0.586	0.676
End-Thrust [kN]	508	552
Active Power [MW]	47.01	47.98
Reactive Power [MVA]	65.00	52.27
Peak Input Power [MVA]	80.22	70.95
Armature mass [kg]	869	8286
Pole pitch [mm]	600	154
Stack width [mm]	2000	2000
Mover length [mm]	4800	4312
Airgap length [mm]	7	7
Aluminum thickness [mm]	20	-
Magnet thickness [mm]	-	49.9
Active pole pairs	3	14
Slot per pole per phase	4	3/7
Current density [A/mm ²]	50	50
Peak Frequency [Hz]	74	278
Thrust density [Pa]	70560	63850

of the input variables. The main outcome of the sensitivity analysis are charts that present in the y-axis the percent variation of an output with respect to its mean and in the x-axis the percent variation of each input variable with respect to its own mean value. The slope of the curves represents the sensitivity of the system to the respective input parameter variation. The selection of the geometrical parameters through the sensitivity analysis approach allows the sizing of the linear electromagnetic launchers to achieve the minimum input power within the design constraints.

The performance of the two machine topologies sized using the sensitivity analysis and presented in this paper is shown in Table II. In particular, LPMSM’s mover presents a much larger mass due to the high density of the magnetic material.

IV. CURRENT DENSITY LIMIT OF THE STATOR WINDINGS

The rated current density on the primary stator windings shown in Table II is considerably higher than the usual limit of electrical machine without active cooling for continuous operation (~ 4 A/mm²) [4]. However, both the machines are formed by several stages each one separately connected to the power supply and fed for a short time. The primary current in each stage flows for a time Δt which includes the time required by the mover to cross the stage itself and the time taken by the machine to develop its magnetic field.

Since the aircraft accelerates during the launch, the time needed to pass each stage is gradually shorter as the motion progresses. Therefore, the primary windings of the first stage will need to be connected to the power supply for the longest period (~ 1.26 s) and will experience the strongest temperature rise.

The time spent to build up the magnetic flux in each stage of the machine depends on the electromagnetic features of the linear motor. Current and magnetic flux reach their rated value after a period that corresponds to approximately five times the time constant of the machine. In a similar way the current takes

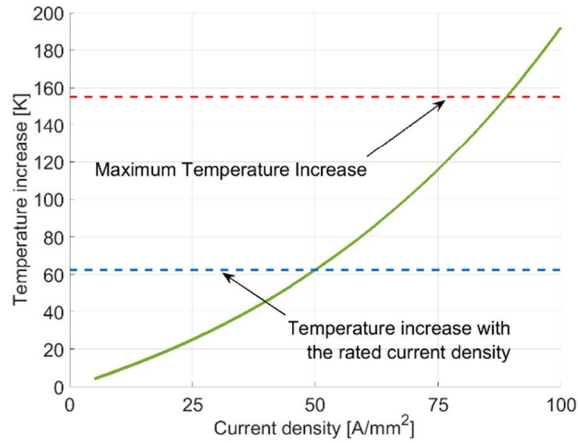


Fig. 3. Primary windings temperature increase with the current density.

around five time constants to return to its initial value. Since the current profile during the flux charging and discharging is complementary, the thermal analysis considers the primary current flowing for only five time constants, but at its full rate. For an inductive/resistive electric circuit, for example the equivalent circuit of the induction motor, the time constant is given by the ratio between the primary inductance and the primary resistance. The secondary inductance is not usually considered in the calculation because for double-sided linear motor its value is close to zero and can be neglected [12].

Thus, the total time the current flows in the first stage can be compute as

$$\Delta t = \sqrt{\frac{2l_{st}}{0.6 \cdot G}} + 5 \frac{L}{R} \quad (4)$$

where l_{st} is the length of the stage, L is the phase inductance, and R the phase resistance.

The temperature increase of the first stage windings can be computed considering the balance over time between the heating due to the electrical energy and the thermal energy gained by the wire material

$$c_{Co} M_{Co} \partial T = R I_1^2 \partial t \quad (5)$$

where c_{Co} is the specific heat capacity of the wire, M_{Co} the mass of the copper, and I_1 the primary current. The integration of the energy balance leads to Onderdonk's law which can be written as [13]

$$\Delta T = (234 + T_i) [10^{33.5(I_1/A_w)^2 \Delta t} - 1] \quad (6)$$

where T_i is the initial temperature and A_w the wire area in circular mils.

The results of (6) solved for several current densities are reported in Fig. 3 where the maximum ΔT allowed by the insulation and the ΔT caused by the rated current density are highlighted. The rated current density $J = 50 \text{ A/mm}^2$ causes the copper wire to increase its temperature by only 62.3 K after a time Δt of 4.35 s, as shown in Fig. 3.

According to the results shown in Fig. 3, the launcher can operate without any active cooling of the stator windings after the first aircraft acceleration. Even though the temperature

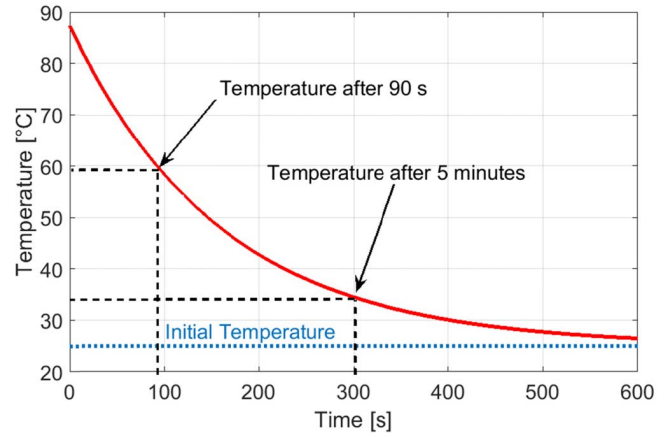


Fig. 4. Temperature evolution of the coil of the first stage after the power supply is disconnected.

raise during a single launch can be handled by the thermal insulation, the launcher has to perform multiple launches to cope with the air traffic of the airport.

In order to model the temperature profile of a coil of the first stage after the current ceases to flow a simple 1-D thermal model is introduced

$$\frac{\partial T}{\partial t} = \frac{k_{ins} S_{wire}}{b_s/2 \cdot \rho_{Co} c_{Co} V_{wire}} (T_i - T) \quad (7)$$

where k_{ins} is the thermal conductivity of the insulation (Mica 0.528 W/m/K), S_{wire} is the external surface of the wire, b_s is the slot width, ρ_{Co} is the copper density, and V_{wire} is the volume of the wire. The analysis is restricted to a single wire since all the turns of a coil behave in a similar fashion. Moreover, the heat transfer model in (7) is only applied to study the temperature evolution of the part of the wire inside a single slot, since the heat flow along the wire length can be neglected. The slowest passive cooling occurs when the wire is located in the middle of the slot with an insulation thickness equal to $b_s/2$, as shown in (7). The integration of (7) for a time span of 10 min yields the result shown in Fig. 4.

Busy airports like Heathrow reach an average number of movements (takeoffs and landings) of about 1300 per day [14]. With this take-off frequency, the time between two consecutive launches may reduce to as little as 90 s during peak times. Within this time the initial coil temperature of 25 °C should be passively or actively re-established. According to the curve shown in Fig. 4, the initial temperature is passively restored after a period longer than 10 min.

The temperature profile shown in Fig. 4 shows that after 90 s the temperature of the coil is 60.5 °C. At this time, another launch would heat the stator windings up to a temperature of approximately 123 °C. However, the hotter is the motor with respect to its environment the faster it exchanges heat with the surrounding. The temperature of the coil T_x at which the heat absorbed during the launch is equal to the heat dissipated through the insulation in 90 s can be computed as

$$T_x = \frac{\Delta T + T_i [1 - \exp(-A \cdot 90)]}{1 - \exp(-A \cdot 90)} \quad (8)$$

where ΔT is the temperature delta computed by (6) and the constant A is calculated as

$$A = \frac{k_{\text{ins}} S_{\text{wire}}}{b_s/2 \cdot \rho_{\text{Co}} c_{\text{Co}} V_{\text{wire}}}. \quad (9)$$

Solving (8) with the geometrical data of the linear induction motor yields an equilibrium temperature of 169.6 °C. Even though the temperature T_x can be handled by high class insulations, the presence of hot spot due to material defects might locally compromise the electrical insulation. Furthermore, the method presented in (8) assumes that each launch causes the same ΔT . The variation of the coil resistivity changes the temperature delta, so that the temperature T_x may exceed the insulation limit leading to the need of an active cooling system.

V. THERMAL ANALYSIS OF LIM

The heat transfer problem has been solved to estimate the temperature evolution in the aluminum plate of the LIM's mover during the launch. The thermal conditions of the material under load may affect the structural response of plate and cause creep. Creep is the tendency of a material to deform permanently under high mechanical stresses and heat loads especially when they are applied for a long time. The rate of deformation depends on the applied temperature, structural load, and exposure time. Creep is observed in all metals, provided that the operating temperature exceeds $k_{\text{cr}} \cdot T_M$, where T_M is the absolute melting temperature and k_{cr} is a coefficient that depends on the material. The melting temperature of aluminum is 933.3 K (660 °C) and the creep coefficient is 0.54 [15]. Under the creep temperature T_{cr} of 504 K (231 °C) creep can be neglected.

The temperature of the solid aluminum changes during the launch because of the heat generation due to the induced current and its variation can be described using

$$\rho_{\text{Al}} c_{\text{Al}} \frac{\partial T}{\partial t} - q_v = \nabla \cdot (k_{\text{Al}} \nabla T) \quad (10)$$

where q_v is the volumetric heat generation due to Joule losses and ρ_{Al} , c_{Al} , and k_{Al} are the aluminum density, specific heat capacity, and conductivity, respectively. The current density J induced in the secondary was extracted from the 2-D transient finite element analysis (FEA) simulation and implemented in the 3-D thermal model. The third dimension of the FEA data is obtained assuming constant current density along the depth of the motor.

The specific Joule losses in the domain are computed from the local current density J and conductivity σ_{Al} as

$$q_v = J^2 / \sigma_{\text{Al}}. \quad (11)$$

Equation (10) is solved using the implicit finite difference method which accounts for the heat exchanged through convection across all the boundaries. The amount of heat that crosses the boundary by convection depends on the relative speed between the solid surface and the surrounding air. The temperature of the solid material and the air physical properties affect the boundary heat transfer as well. The convective coefficient expresses the heat transfer between a solid surface

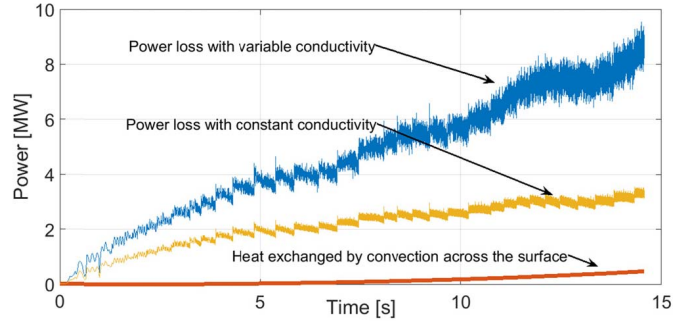


Fig. 5. Variation of the secondary Joule losses with time.

and a fluid and takes into account of the state of the fluid and solid media. In an EML system the mover changes speed and its temperature varies because of the Joule losses in the system. In order to correctly describe the instantaneous state of the moving plate the value of the convective coefficient has to be updated according to the change of the system parameters.

The resistance of a conductor to a current flow is the result of the collision between the current electrons and crystallographic structure of the conductor. The temperature of a solid material represents the amplitude of the oscillation of the atoms around their average position in the inner structure. When the oscillations amplitude increases the chances of a collision with the electrons of a current flow also increases. The results is a increment of the conductor resistivity ρ_c according to the law

$$\rho_c = \rho_0 [1 + \alpha_c (T - T_0)] \quad (12)$$

where α_c is the temperature coefficient of resistance and ρ_0 is the resistivity at the temperature T_0 . The increment of resistivity and of respective Joule losses is taken into account during the solution of the heat transfer problem. Fig. 5 compares the Joule losses computed by the thermal analysis software with variable resistivity with those computed by the FEA software with constant resistivity. Fig. 5 also shows the total heat exchanged at the boundary through convection.

The solution of the heat transfer problem given in (10) yields the time evolution of the temperature over the aluminum plate volume. The skin effect causes the current density to gather close to the aluminum boundary as the frequency increases during the launch. Therefore, the external layer of the aluminum plate is subject to the most severe thermal conditions. The temperature profile on the lateral surface of the mover is captured at different time instants shown in Fig. 6. The maximum temperature is reached at the end of the launch after 14.57 s, as shown in Fig. 6. The creep temperature is never reached, as 499.7 K is the maximum temperature obtained on the plate surface. Even though the maximum temperature is close to the creep point, it is reached on a very small area, whereas the average temperature of the mover at the end of the launch is 442.9 K.

Although the additional losses due to the resistivity variation increase, these results demonstrate that the thermal requirement for the aluminum plate is satisfied. Therefore, the launcher can safely operate under the thermal load without

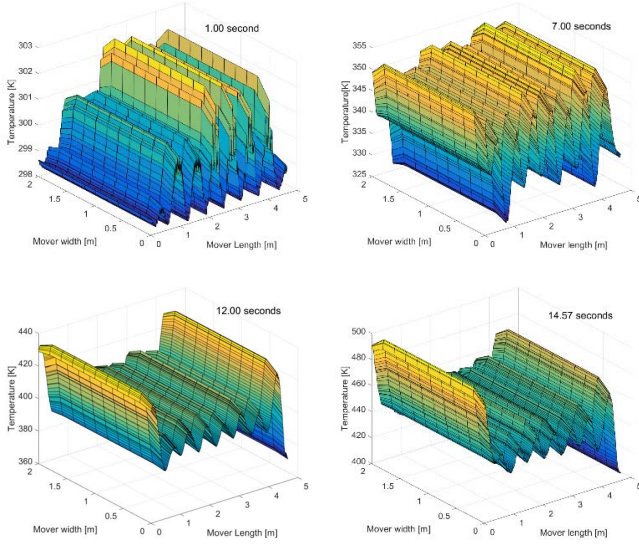


Fig. 6. Temperature profile on the mover surface that faces the stators at different time instants during the launch.

permanent deformations due to the creep of material, even without an active cooling system. Nevertheless, when the effect of multiple launches is considered, the temperature on the mover would gradually build up unless the aluminum plate has enough time to passively cool down to the initial temperature or unless it reaches the equilibrium between the heat absorbed during the launch and the heat dissipated through convection. Since the peak temperature computed by the 3-D thermal analysis is very close to the creep point of the material (504 K), any additional launch would cause creep to occur before reaching any heat equilibrium. An active cooling system might be required to bring the plate to its initial temperature before the next launch.

VI. THERMAL ANALYSIS OF LPMSM

The transient heat transfer problem for the LPMSM mover's yoke might be solved adopting the same techniques exploited to determine the temperature transient of the LIM's secondary. However, in this case a 3-D transient thermal analysis is not required for the following reasons.

- 1) Since the mover is synchronized with the magnetic wave, the eddy currents are induced only by the secondary harmonics. In the LIM the currents induced in the aluminum plate are mainly due to the fundamental wave and the current density reaches higher intensities.
- 2) The eddy current intensity is further reduced by the low conductivity of the stainless steel.
- 3) The LIM's aluminum plate is located in proximity to the primary windings where the magnetic flux oscillations are more intense. The stainless steel yoke of the LPMSM is located behind the magnets at a larger distance from the stator coils.
- 4) Creep becomes a dominant effect when the temperature of the stainless steel exceeds the limit $T_{cr} = 0.49 \cdot T_M$ where the melting temperature T_M of the material is

1723 K (1450 °C). Therefore, the creep temperature limit of stainless steel is about 844 K (571 °C) which is much higher than temperature limit of aluminum (504 K or 231 °C). Creep is not expected to occur in the yoke material, especially considering that magnets in contact with steel at such a temperature would lose any trace of magnetization.

- 5) In the hypothesis of perfect thermal insulation between the magnets and the yoke, conduction occurs only between the active area and the passive area of the mover (mover overhangs connected to aircraft and to the guidance systems). To further simplify the problem, the analysis is restricted only to the active area where the eddy currents are generated. At the fictitious boundary surfaces between the active and passive area perfect thermal insulation is imposed. Since the passive area is always colder than the active area, with this assumption the heat that flows across the boundary between the active and passive zone is neglected and the temperature in the active region will be higher than in real applications.
- 6) Under the previous assumption, the convective heat flows only through the leading edge surface and the trailing edge surface of the active area, since the lateral surfaces are covered by the PMs. Since the heat removed through convection along these surfaces is not significant, convection can be neglected. Perfect thermal insulation is then also imposed along the mover leading and trailing surfaces.
- 7) As will be further discussed later, heat conduction between the yoke and the magnets is neglected. This assumption does not correspond to what happens in the real application, but it greatly simplifies the analysis without leading to significant errors as far as the temperature delta is limited to a few degrees.

The transient heat transfer equation for the yoke under these assumptions reduces to

$$\rho_{ir} c_{ir} \frac{\partial T}{\partial t} = \frac{P_{yoke}(t)}{V_{yoke}} \quad (13)$$

where ρ_{ir} is material density, c_{ir} is the material specific heat capacity, V_{yoke} is the volume of the mover's yoke and P_{yoke} is the power which is dissipated as heat into the yoke. The time variation of the Joule losses in the stainless steel during the launch was computed through FEA and it is shown in Fig. 7.

The integration of both sides of (14) over the take-off time t_{TO} yields

$$\Delta T_{yoke} = \frac{1}{\rho_{ir} c_{ir} V_{yoke}} \int_0^{t_{TO}} P_{yoke}(t) dt \quad (14)$$

where ΔT_{yoke} is the average temperature increment.

Integrating the power loss in Fig. 7 yields a temperature difference of approximately 11.6 K. This temperature delta does not represent an issue during a single launch, but a cooling system might be required for multiple consecutive launches. Indeed the heat removed by convection across the yoke surfaces is little, and the mover will take several hours to return to the initial condition even with such a

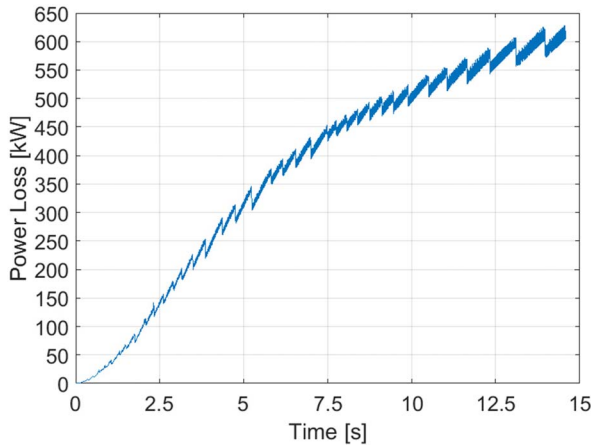


Fig. 7. Transient variation of the Joule losses in the mover's yoke during the launch.

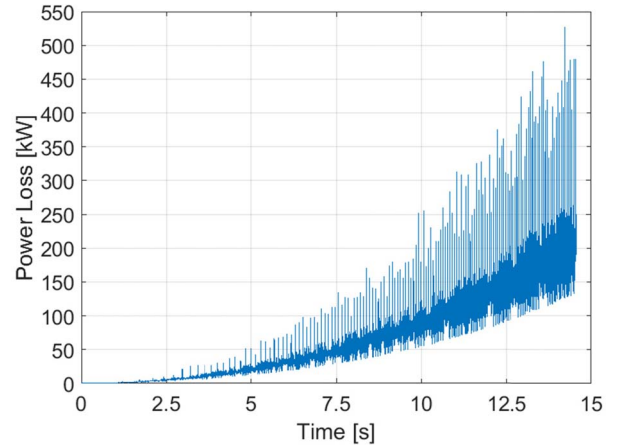


Fig. 8. Transient variation of the eddy current losses in the surfaced-mounted PM array.

small temperature increase. However, within the time between launches the passive cooling provided by conduction across mover overhangs and across the magnets will allow several consecutive takeoffs without the need for any cooling system.

The thermal heat transfer model is also applied to determine the temperature change of the surface-mounted magnets during the launch, to prevent demagnetization. Demagnetization may be caused by eddy currents induced by the secondary harmonics of the magnetic wave. The intensity of secondary harmonics is particularly significant in a fractional-slot motor like the synchronous launcher under investigation.

A technique that is widely used to reduce the loss in the magnets consists in shortening the eddy current path by segmentation. Each magnet can be segmented in both axial and longitudinal directions. Fifty axial and four longitudinal magnet segmentations were implemented to limit the intensity of the induced eddy current.

Since the eddy current losses in each pole of the magnet array are almost equal, the thermal analysis of the magnets can be restricted to a single pole. Moreover the axial segmentation allows the investigation of the temperature transient of a single internal segment. Considering that neighbor magnet segments undergo approximately the same temperature rise and that the interstices between magnets are filled with a low thermal conductivity glue, the sides of each magnet segment can be considered perfectly thermally insulated. Neglecting the heat exchanged through convection over the small surface exposed to air and the heat conduction to the yoke, the heat transfer problem can be solved analytically by applying

$$\rho_{PM} c_{PM} \frac{\partial T}{\partial t} = \frac{P_{PM}(t)}{V_{PM}} \quad (15)$$

where ρ_{PM} is the magnetic material density, c_{PM} is the permanent magnets specific heat capacity, V_{PM} is the volume of the magnet segment, and P_{PM} is the power loss in a magnet segment.

The loss due to eddy current in the array of magnets that covers the mover is shown in Fig. 8. The spikes in Fig. 8 are due to the brisk flux variation that occurs when the mover passes from one stage to another. The power loss in Fig. 8

refers to the full PM array on both sides of the mover's yoke, whereas the loss P_{PM} in (15) refers to a single axial segment. The longitudinal segmentation of each magnet pole is neglected by the thermal problem since it does not affect the final solution.

The increase of the magnet average temperature can be calculated solving (15) as

$$\Delta T_{Mag} = \frac{1}{\rho_{PM} c_{PM} V_{PM}} \int_0^t P_{PM}(t) dt. \quad (16)$$

The integration of (16) yields a temperature rise of 0.37 K which is manageable by passive cooling even in the hypothesis of multiple launches.

VII. RESULTS AND CONCLUSION

The optimization of the electromagnetic performance of an EML alone does not lead to a viable configuration for a civil aircraft application without thermal validation of the design. For instance, the thermal analysis of the coils of the first stage of the linear induction motor presented in Section IV showed that without active cooling the temperature would gradually rise above the insulation limit as a consequence of multiple launches and resistivity increase. The extra heat should be actively removed with the aid of fans located along the track. Since the mover takes the longest time to cross the first stage, the current will not heat the windings of all the other stages in the same way and the actual motor configuration will require an active cooling system only along the first part of the track. In order to prevent the use of an active cooling system, the electromagnetic design should be modified to allow lower rated current density to flow in the first stages of the machine.

The thermal analysis of the LIM's mover presented in Section V has crucial importance in the selection of the proper value of the aluminum thickness, which is proportional to the plate thermal capacity. Shorter aluminum thickness would increase the electromagnetic performances, but would rise the plate temperature above the creep limit. The aluminum thickness that was selected for LIM's mover is large enough

to prevent sharp temperature rise and plastic deformation due to the creep of the material.

It may be argued that an active cooling system might be used to remove the additional heat losses in order to keep the value of the aluminum resistivity constant and further reduce the plate thickness. However, a cooling system that acts on a moving object along the track is impractical and difficult to implement. An alternative method that can be exploited to maintain the aluminum resistivity around the desired value is by cooling the plate at liquid nitrogen temperature before the launch. The resistivity would eventually rise, but not to the point reached without any precooling.

In order to cope with multiple launches, the mover has to be actively cooled down to environmental temperature after each launch. Unlike the primary coils studied in Section IV, the mover for the next takeoff can be different from the one used in former launch. Every mover can be reused as soon as the initial temperature is passively restored without the need of a cooling system, but this solution will increase the system complexity.

The thermal analysis of LPMSM presented in Section VI showed that surfaced-mounted magnets do not suffer from thermal demagnetization even after multiple launches as long as longitudinal and axial segmentation is applied appropriately. Since the temperature increase in a magnet segment is very little and magnet lamination increases cost and installation complexity, the selected number of axial and longitudinal segments can be reduced.

The component of the LPMSM's mover that experiences the greatest temperature rise is the stainless steel yoke. The temperature difference between yoke and magnets generates a heat flow that tends to cool down the yoke and heat up the magnets. However, the low conductivity of the glue used to stick the magnets on the mover's yoke and the short duration of the launch impede the attainment of thermal equilibrium during the acceleration and the temperatures of the mover's components are not expected to vary much from the values found in the presented simplified analysis. At the same time the temperature difference between yoke and magnets does not generate heat flows that strongly affect the temperature distribution on the mover during the launch. The implementation of a yoke with axial segmentations might further reduce the eddy current loss in the material and completely remove the need for active cooling, even with many consecutive launches separated by a short time span.

In conclusion, if only a passive cooling system is desired along the track of LIM, the electromagnetic design methodology that determines the parameters of the motor in Table II, must be combined with the thermal analysis to select the rated current density of each stage and the mover thickness. Although the aluminum plate withstands the temperature increase caused by a single launch, an active cooling system is needed to cool down the mover at the end of the acceleration to cope with multiple launches.

On the contrary, the electromagnetic design procedures used to size the LPMSM defined in Table II lead to a machine configuration which is also particularly efficient from the thermal point of view. A passive cooling system will suffice to keep PMs and mover yoke at the desired temperature even with several consecutive launches. The stator windings of the LPMSM do not suffer the same temperature increase of LIMs for the shorter time constants: reduced inductance and comparable resistance in (4). Therefore, the rated current density can be applied to the LPMSM's stator windings without any particular precaution.

REFERENCES

- [1] G. Bellamy and E. Lewis, "The development of advanced linear induction motor systems," in *Proc. Power Electron. Mach. Drives*, Edinburgh, Scotland, Apr. 2004, pp. 873–878.
- [2] A. Musolino, R. Rizzo, and E. Tripodi, "The double-sided tubular linear induction motor and its possible use in the electromagnetic aircraft launch system," *IEEE Trans. Plasma Sci.*, vol. 41, no. 5, pp. 1193–1200, May 2013.
- [3] D. Patterson *et al.*, "Design and simulation of a permanent-magnet electromagnetic aircraft launcher," *IEEE Trans. Ind. Appl.*, vol. 41, no. 2, pp. 566–575, Mar. 2005.
- [4] D. G. Dorrell, M. Hsieh, M. Popescu, L. Evans, D. A. Staton, and V. Grout, "A review of the design issues and techniques for radial-flux brushless surface and internal rare-earth permanent-magnet motors," *IEEE Trans. Ind. Electron.*, vol. 58, no. 9, pp. 3741–3757, Sep. 2011.
- [5] Y. Zhang, J. Ruan, T. Huang, X. Yang, H. Zhu, and G. Yang, "Calculation of temperature rise in air-cooled induction motors through 3-D coupled electromagnetic fluid-dynamical and thermal finite-element analysis," *IEEE Trans. Magn.*, vol. 48, no. 2, pp. 1047–1050, Feb. 2012.
- [6] GENERAL ATOMICS. (Oct. 2014). *EMALS*. [Online]. Available: <http://www.ga.com/emals>
- [7] B. Schweber. EDN Magazine. (Apr. 11, 2002). *Electronics Poised to Replace Steam-Powered Aircraft Launch System*. [Online]. Available: <http://www.edn.com/design/analog/4341471/Electronics-poised-to-replace-steam-powered-aircraft-launch-system>
- [8] L. Bertola, T. Cox, P. Wheeler, S. Garvey, and H. Morvan, "Reducing weight and fuel consumption of civil aircraft by electromagnetic launch," *Int. J. Mech. Aerosp. Ind. Mechatron. Manuf. Eng.*, vol. 11, no. 2, pp. 225–229, 2017
- [9] *Standard Practice for Design of Amusement Rides and Devices*, ASTM F2291-13, West Conshohocken, PA, USA, 2014.
- [10] *Airport Commission: Final Report*, AIRPORT. COMMISSION, London, U.K., 2015.
- [11] L. Bertola, T. Cox, P. Wheeler, S. Garvey, and H. Morvan, "Electromagnetic launch systems for civil aircraft assisted take-off," *Arch. Electr. Eng.*, vol. 64, no. 4, pp. 543–554, 2015.
- [12] I. Boldea, *Linear Electric Machines, Drives, and MAGLEVs Handbook*. Boca Raton, FL, USA: CRC Press, 2013.
- [13] E. R. Stauffacher, "Short-time current carrying capacity of copper wire," *General Elect. ric Rev.*, vol. 31, no. 6, pp. 326–327, 1928.
- [14] HEATHROW COMPANY. (Dec. 2016). *Heathrow Company: Facts and Figures*. [Online]. Available: <http://www.heathrow.com/company/company-news-and-information/company-information/facts-and-figures>
- [15] S. Spigarelli, "Creep of aluminium and aluminium alloys," in *TALAT Lecture 1253*, Eur. Aluminium Assoc., [Online]. Available: <http://core.materials.ac.uk/repository/ea/talat/1253.pdf>

Authors' photographs and biographies not available at the time of publication.